

FINAL REPORT
Classification and High-Resolution Delineation
of the Fire-Prone Wildland-Urban Interface
JFSP PROJECT ID: 22-1-01-6

APRIL 2025

Megan E. Cattau
Boise State University

Megan R. Dolman
Boise State University



FIRESCIENCE.GOV
Research Supporting Sound Decisions



Table of Contents

Acknowledgements.....	3
Keywords.....	3
List of Tables.....	3
List of Figures.....	3
List of Abbreviations/Acronyms.....	3
Abstract.....	5
1. Objectives.....	5
2. Materials and Methods.....	6
2.1 Mapping Built Infrastructure.....	6
2.1.2 Satellite Imagery.....	10
2.1.2 Classification.....	12
2.1.3 Accuracy Assessment and Validation.....	12
Time Series Analysis and Product Comparison.....	13
2.2 Wildland-Urban Interface Mapping.....	14
3. Results and Discussion.....	14
3.1 Mapping Built Infrastructure.....	14
3.2 Wildland-Urban Interface Mapping.....	18
Conclusions and Implications for Management/Policy and Future Research.....	18
Literature Cited.....	18
Appendix A: Contact Information for Key Project Personnel.....	18
Appendix B: List of Completed/Planned Scientific/Technical Publications/Science Delivery...	19
Table 3. Deliverables and products with description and status.....	19
Appendix C: Metadata.....	20

List of Tables

Table 1. Land use land cover (LULC) product classes and definitions. Class definitions for NLCD (“National Land Cover Database Class Legend and Description | Multi-Resolution Land Characteristics (MRLC) Consortium,” n.d.) and DW (Brown et al., 2022) are taken directly from product descriptions.

Table 2. Spectral Indices.

List of Figures

Figure 1. (a) Snake River Plain, Idaho, and the Region of Interest (ROI) reference data locations. (b-c) National Agriculture Imagery Program (NAIP) false color composites (Near Infrared (NIR), red, green) of ROIs (Owyhee (b), and Teton (c)). Our classification was completed across the Snake River Plain.

Figure 2. Open-source software workflow for mapping built infrastructure in semi-arid systems, including reference data generation, classification, accuracy assessment and validation.

Figure 3. Comparing NAIP aerial imagery to digitized polygons for each LULC class in our workflow ((a) Residential, (b) Infrastructure, (c) paved, (d) Agriculture, (e) Vegetation, (f) Range/Scrub).

Figure 4. Comparing spatial, temporal and thematic resolutions of existing LULC products to our mapped built infrastructure (MBI) products. Both DW and MBI have a spatial resolution of 10 m and thus have an identical pixel size, but these products differ in their thematic resolution. The higher thematic resolution of MBI is illustrated by the three hatched shapes within the black square; however, these do not represent sub-pixel features, but rather serve as a schematic to demonstrate the enhanced thematic detail of our product, compared to the single ‘built’ class in DW. Likewise, the four hatched shapes within the NLCD represent the four ‘developed’ classes.

Figure 5. Classification results for the year 2024 across the Snake River Plain (SRP), and comparisons between 2016 and 2024 classifications in (a) Boise (west SRP), (b) suburbs to the north of Twin Falls (south SRP), and (c) Ammon, a suburb city to the east of Idaho Falls (east SRP).

Figure 6. Comparing class areas (km²) across the SRP as mapped by different LULC products, including our mapped built infrastructure (MBI) product, global Dynamic World (DW), Microsoft Building Footprints (MBF), and National Land Cover Dataset (NLCD). 2023 values for the NLCD Low Intensity class were surprisingly high, with a 161% increase in area for this particular class, from 697 km² in 2021 to 1816 km² in 2021. Released in October 2024, the 2023 NLCD data mostly compare well with previous years, however this increase seems questionable. As such, we have omitted the NLCD Low Intensity class and Built SUM for the year 2023.

Figure 7. Spatial comparison of classes between (a) our mapped built infrastructure, (b) Microsoft Building Footprints (MBF) (c) National Land Cover Dataset (NLCD) and (d) Dynamic World (DW) for the year 2021.

List of Abbreviations/Acronyms

AI: Artificial Intelligence
BSI: Bare Soil Index
BUI: Built-Up Index
CART: Classification and Regression Tree
CE: Commission Error
DW: Dynamic World
FAIR: Findability, Accessibility, Interoperability, Reusability
GEE: Google Earth Engine
GRD: ground range detected
H: horizontal
IDL: Idaho Department of Lands
LULC: land use and land cover
MBF: Microsoft Building Footprints
MBI: Mapped built infrastructure
NAIP: National Agriculture Imagery Program
NBAI: Normalized Built-Up Area Index
NBI: New Built-Up Index
NDBI: Normalized Difference Built-Up Index
NDVI: Normalized Difference Vegetation Index
NED: National Elevation Dataset
NIR: near infrared
NLCD: National Land Cover Database
NRT: near real-time
OA: Overall Accuracy
OE: Omission Error
PA: Producer's Accuracy
QGIS: Quantum Geographic Information System
RF: Random Forest
RI: Road Index
ROI: region of interest
SAR: Synthetic aperture radar
SRP: Snake River Plain
SVM: Support Vector Machine
SWIR: short-wave infrared
TOA: top of atmosphere
UA: User's Accuracy
UI: Urban Index
US: United States
USDA: United States Department of Agriculture
USGS: United States Geological Survey
V: vertical
WUI: wildland-urban interface

Acknowledgements

We acknowledge that this research was funded by the Joint Fire Science Program under the Graduate Research Innovation (GRIN) Project JFSP award number: FA-FOA0022-001. JFSP GRIN funding allowed us to expand existing research funded by the Idaho-wide *Genes to Environment: Modeling, Mechanisms, Mechanisms, and Mapping (GEM3)* project, funded through the National Science Foundations' Idaho Established Program to Stimulate Competitive Research (EPSCoR) under award number OIA-1757324. This JFSP-funded expansion supported engagement with the Idaho Department of Lands, and specifically we thank Tyre Holfeltz for his enthusiastic support and consultation that contributed greatly to this report. We also thank the following research assistants for their assistance in generating the reference data: Savannah Canova, Andrew Cesca, Zackery Szymczycha, Karla Rogers, Adrianna Hernandez, Alexandria Serbellon, Micaela Gonzalez, Jacob Scott, Samantha Yonan, Tyler Zafiris and Will Loftin. We also thank the broader GEM3 community, the GEM3 Stakeholder Advisory Groups, Peter Olsoy, and Morey Burnham. Thanks too goes to our co-authors on our peer-reviewed paper describing the MBI products: Rebecca Som Castellano, Trevor Caughlin, and Jodi Brandt.

Keywords

remote sensing, image classification, built-up indices, urban mapping, cloud computing, Google Earth Engine, time series

Abstract

Human population growth is driving the expansion of infrastructural development into the fire-prone Wildland-Urban Interface (WUI). Infrastructural development in the WUI alters fire processes, both by altering vegetation - which can be fuel for fire - and by introducing more ignitions. The proximity of human infrastructure to vegetation fuels is unique to the WUI. Fire activity, fire hazard risk and exposure is highly problematic in WUI systems, but is not exclusive to WUI systems. Across the Western US, WUI expansion is concurrent with shifting fire regimes, characterized by increasing size, frequency, severity, and season length, in addition to growing human ignitions. Yet both WUI and non-WUI communities must adapt to these changes as fire activity can be unpredictable, and fire hazards are not unique to the WUI. Adapting to changing fire activity and reducing human exposure to fire hazards in both WUI and non-WUI requires a more comprehensive understanding of the spatial-temporal dynamics between built infrastructure and fire processes.

Addressing these issues requires infrastructure data that are well-mapped at an annual temporal resolution to track change over time. However, existing data omit critical information to capture trends accurately due to temporal, spatial, and thematic resolution limitations. The lack of finer-scale data inhibits our ability to develop targeted and effective tools and limits decision making and management strategies regarding human exposure, mitigation, and adaptation to wildfire in the WUI. Advancements in remote sensing imagery, open-source software and cloud computing offer opportunities to address these challenges.

Using Google Earth Engine, we developed a novel built infrastructure detection method in semi-arid systems by applying a random forest classifier to a fusion of Sentinel-1 and Sentinel-2 time series. Our classifier performed well, differentiating three built environment types: residential, infrastructure, and paved, with overall accuracies ranging from 90-96%. Sentinel-1 variables were important for differentiating built classes. We illustrated the utility of our mapped products by generating a time-series of change across southern Idaho spanning 2015 to 2024 and comparing this with publicly available products: National Land Cover Database (NLCD), Microsoft Building Footprints (MBF) and the global Dynamic World (DW). Our mapped built infrastructure (MBI) products offer enhancements over NLCD spatially and temporally, over DW thematically, and over MBF both temporally and thematically. We demonstrate the potential of fusing data sources to improve LULC mapping and present a case for regionally parameterized models that can more accurately capture built infrastructure and WUI change over time. In tandem with data analysis, our finer-scale data products will allow for better analysis of fire hazard risk and exposure and fuels management.

1. Objectives

The aim of this project was to demonstrate an open-source approach for mapping built infrastructure in a semi-arid system using remote sensing data and leveraging cloud computing through GEE, to inform WUI fire management, mitigation and adaptation strategies and address the question: **How do finely resolved contemporary patterns of infrastructural development in the WUI influence human exposure to wildfire?**

We applied our methodology to the Snake River Plain (SRP) Level III Ecoregion in southern Idaho, as delineated by the US Environmental Protection Agency (Omernik and

Griffith, 2014). The SRP is an ideal study system for this work owing to the high rates of built infrastructure expansion in recent years, notably in the Boise area, and the associated widespread decline of imperiled sagebrush steppe. We integrated Sentinel-2 imagery with ground range detected (GRD) data collected from the C-band SAR satellite, Sentinel-1. To our knowledge, no workflows have been developed for extracting built infrastructure in semi-arid systems using a remote sensing data fusion. Integrating radar with multispectral imagery has been found to improve the accuracy and effectiveness of image classifiers, and thus demonstrates the potential of fusing numerous data sources to advantage LULC mapping broadly, including for built infrastructure mapping. Our final data products map landscape-scale built infrastructure at an annual temporal resolution for the time series 2015-2024. We: (1) applied detection algorithms to publicly-available remote sensing data and generated annually-resolved mapped products of built infrastructure, (2) derived a time series of change across the SRP, with which we demonstrated product application by quantifying changes observed and exploring spatial patterns of built infrastructure within the SRP, and (3) spatially and visually compared our time series with publicly available products, namely NLCD, MBF and DW and discussed their broader utility.

We utilized freely available and open source software to make our workflow and products more accessible for people not only in the scientific community, but those in policy, planning, management, and communities broadly, in addition to our community partner, the Idaho Department of Lands (IDL). Our project addresses the need for comprehensive, mapped data on human built infrastructure to meet the challenges of infrastructure encroaching into fire-prone wildland vegetation systems. Our work to fill this gap is a necessary contribution towards broader efforts to foster resilience for local communities and ecosystems and it is critical owing to shifting fire regimes concurrent with accelerating population growth and infrastructural development expansion. Our work will contribute to improved equity in response to fire hazards, ultimately building sustainable capacity across the Intermountain West and the US broadly.

Accurate, timely built infrastructure maps that differentiate between residential and commercial infrastructure have wide-reaching applications. From the perspective of wildfire risk management and reducing community exposure to wildfire, it can be helpful to know whether a building is occupied or not. Through this research, it became apparent that, while human exposure to wildfire may be more likely in the WUI, it is not exclusive to the WUI. Through a thorough literature review, we found that there is a knowledge gap around understanding of how WUI delineations impact and inform wildfire risk management, which has implications for human community exposure to wildfire. Initially we set out to derive another WUI map from our MBI products. Instead, we chose to critically review how WUI delineations and conceptualizations are informing wildfire risk management and decision-making. Too often, wildfire risk management and decision-making around human community exposure to wildfire hazards is focused on WUI areas only. However, non-WUI areas may also have higher wildfire risk and higher wildfire hazard potential. Our MBI products cover both WUI and non-WUI areas, and could be used to better inform wildfire risk management across WUI and non-WUI areas for improved resource allocation and community prioritization. Through our critical review of WUI conceptualizations in the context of wildfire risk management, we emphasize that both standardized and place-based WUI definitions have value, but for different purposes. In the context of wildfire-risk management, more specific, place-based definitions should be used to generate finer spatial resolution WUI maps. Such place-based WUI maps should be used in tandem with other remotely-sensed derived products, infrastructure products like MBI, or vegetation products, to collectively inform wildfire risk management across both WUI and non-WUI areas, rather than the sole focus on WUI delineations.

2. Materials and Methods

2.1 Mapping Built Infrastructure

With the support of the JFSP GRIN, we were able to expand our preliminary analysis from two regions of interest (ROI) subsets of the SRP to the entire SRP (Figure 1). Using QGIS, we manually digitized high resolution aerial imagery, available from the National Agriculture Imagery Program (NAIP) for the two ROIs, one in Owyhee County and one in Teton County (Figure 1b and c), comprising a total area of 3,577 km². NAIP aerial imagery is acquired on a three year cycle at a 1 m resolution. The process of manually digitizing data is very time-consuming and therefore our two digitizing ROIs are relatively small in extent to accommodate for this; however, the spatial resolution of our digitized vector products is very high. The locations of our NAIP reference data collection, Owyhee and Teton, corresponded with two distinct patterns of development and undeveloped wildland vegetation. Teton is dominated by agriculture with dispersed clusters of high-density built infrastructure (Figure 1c), whereas Owyhee is characterized by extensive shrubland, with low-density built infrastructure interspersed between agricultural land (Figure 1b). Residents in both areas have expressed concern over recent built infrastructure expansion and projected future expansion into the fire-prone sagebrush steppe (Netherton-Morrison et al., 2023).

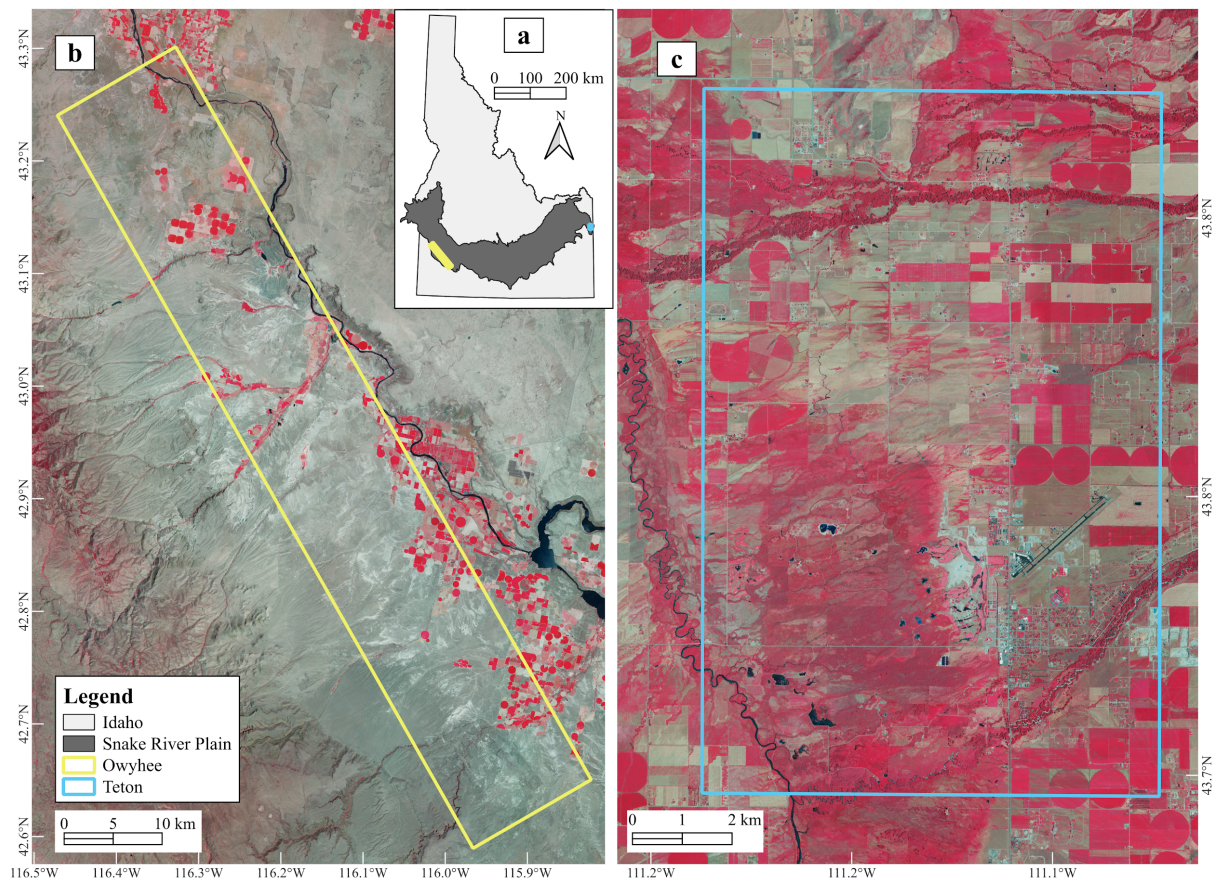


Figure 1. (a) Snake River Plain, Idaho, and the Region of Interest (ROI) reference data locations. (b-c) National Agriculture Imagery Program (NAIP) false color composites (Near Infrared (NIR), red, green) of ROIs (Owyhee (b), and Teton (c)). Our classification was completed across the Snake River Plain.

We mentored and trained eleven research assistants in both QGIS and the digitizing process for training data generation, after which we completed the image classification, accuracy assessment, and time series analysis (Figure 2). Each research assistant was either paid or received academic credit for their time. We recognize that having a greater number of digitizers can be a key source of mis-estimation, which can impact the quality of the reference dataset (McRoberts et al., 2018). To reduce this bias, we trained each digitizer with an identical thorough digitizing protocol and workflow, and we required each trainee to practice the digitizing process before generating reference data for a given ROI and year of NAIP imagery. We checked in regularly with the research assistants to carefully monitor their progress and digitizing style and were available to clarify any uncertainties throughout the process. Before using these data for algorithm training, we spot-checked each students' finished vector data in QGIS to see if their class assignments matched with our class assignments. We then used the *dplyr* and *tidyverse* packages in R to clean the class labels, remove any spelling errors, and assign each class an ID number for use in GEE (Figure 2) (Wickham et al., 2023, 2019).

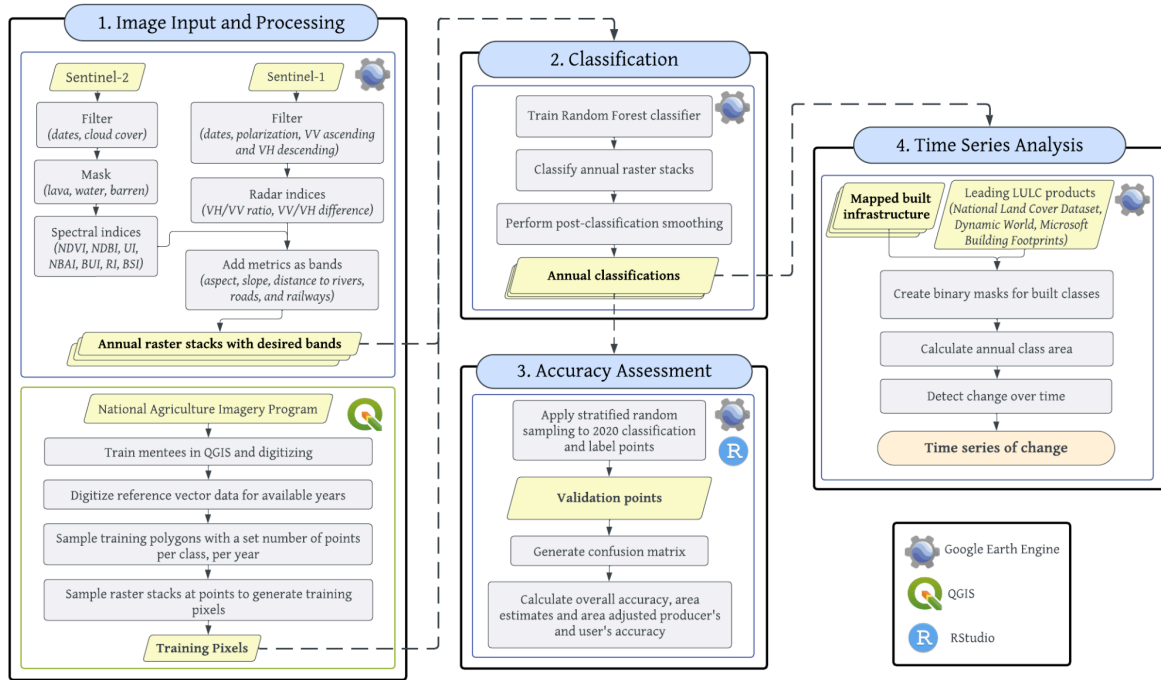


Figure 2. Open-source software workflow for mapping built infrastructure in semi-arid systems, including reference data generation, classification, accuracy assessment and validation.

Our final digitized vector data have a thematic resolution of six classes: five representing land cover modified by human activity (residential, infrastructure, roadway, agriculture, and vegetation), and one representing natural land cover (range/scrub) (Table 1; Figure 3), for the years 2015, 2017, 2019 and 2021. To improve upon the broad definitions of built and urban environments used in existing products, we selected 3 classes representing built infrastructure types: residential, infrastructure and roadway. Our aim of including more nuanced urban environment definitions was to differentiate residential dwellings from other infrastructure types and result in more informed LULC and WUI maps.

Table 1. Land use land cover (LULC) product classes and definitions. Class definitions for NLCD (“National Land Cover Database Class Legend and Description | Multi-Resolution Land Characteristics (MRLC) Consortium,” n.d.) and DW (Brown et al., 2022) are taken directly from product descriptions.

Dataset	Class (Class ID)	Definition
Mapped Built Infrastructure (MBI)	Residential (1)	A human-built structure that represents a place of residence or clear domicile, including mobile homes
	Infrastructure (2)	A human-built structure or human-built object that is not a place of residence, i.e. buildings that are not considered house (barns, silos, sheds, storage units, etc.) and other infrastructure (such as electric power stations, wind turbines, oil well, railway tracks, highways, construction sites, natural resource extraction, and farming structures)
	Paved (3)	An area that includes paved roads covered with asphalt or concrete (parking areas both commercial and residential, old foundations), can include some unpaved roads, including dirt and gravel roads, and dirt trails
	Agriculture (4)	An area that has been cleared of natural vegetation for the cultivation of crops, identified by the presence of row crops, farming equipment, hay bales, irrigation equipment, and fallow land
	Vegetation (5)	Planted vegetation, including grass/lawn/turf that is manicured (surrounding homes, etc.), as well as natural vegetation; riparian and trees
	Range/Scrub (6)	Uncultivated grassland, shrubland, shrub-steppe, and desert scrub occupied by herbaceous vegetation and shrubby vegetation
National Land Cover Database (NLCD)	Developed, Open Space (21)	Areas with a mixture of some constructed materials, but mostly vegetation in the form of lawn grasses. Impervious surfaces account for less than 20% of total cover. These areas most commonly include large-lot single-family housing units, parks, golf courses, and vegetation planted in developed settings for recreation, erosion control, or aesthetic purposes
	Developed, Low Intensity (22)	Areas with a mixture of constructed materials and vegetation. Impervious surfaces account for 20% to 49% percent of total cover. These areas most commonly include single-family housing units
	Developed, Medium Intensity (23)	Areas with a mixture of constructed materials and vegetation. Impervious surfaces account for 50% to 79% of the total cover. These areas most commonly include single-family housing units
	Developed, High Intensity (24)	Highly developed areas where people reside or work in high numbers. Examples include apartment complexes, row houses and commercial/industrial. Impervious surfaces account for 80% to 100% of the total cover



Figure 3. Comparing NAIP aerial imagery to digitized polygons for each LULC class in our workflow ((a) Residential, (b) Infrastructure, (c) paved, (d) Agriculture, (e) Vegetation, (f) Range/Scrub).

From within our 10263 training polygons, we generated 15,000 random points for each class for the four years of training data (2015, 2017, 2019 and 2021), producing a total of 360,000 points. At each point, we sampled pixels from our image stacks to produce our final training pixel dataset, which consisted of 201,999 pixels in the sample pool.

2.1.2 Satellite Imagery

We initially proposed using multispectral high-resolution imagery from the Quickbird (2001-2015) and Sentinel-2 satellites (2015-present). We encountered challenges trying to acquire the Quickbird imagery, in part owing to the issues in extent, availability, and reliability of older satellite data. As an alternative to Quickbird, we chose to incorporate Sentinel-1 synthetic aperture radar (SAR) to improve the accuracy of our products.

Using GEE, we acquired Sentinel-2 imagery, which we filtered, masked and used to calculate spectral indices. The atmospherically corrected Harmonized Sentinel-2 Level 2A surface reflectance (SR) accessible in GEE is only available from 2017 to 2024. As we required SR for the time series 2015 to 2024, we converted the Harmonized Sentinel-2 Level 1C top of atmosphere (TOA) reflectance to SR using the Sensor Invariant Atmospheric Correction (SIAC) (Javed et al., 2021; Yin, 2024). To ensure that each image stack was treated identically, we performed these atmospheric corrections for every year, including those where SR was accessible through GEE. For each year we filtered for imagery collected between the months of June and September. These images include four bands delivered at 10 m resolution (blue, green, red, near infrared (NIR)), and a further six bands delivered at 20 m resolution (three red edge bands, a narrow NIR band, and two short-wave infrared bands (SWIR)). We first restricted our analyses to images that contained less than 30% clouds, and then applied the Sentinel-2: Cloud Probability threshold, set at 20%, to mask clouds present in these images.

A variety of spectral indices are increasingly employed in built infrastructure mapping to enhance feature separability between urban and non-urban areas in images. We chose to include eight spectral indices in our model (Table 2) (Javed et al., 2021; Lynch et al., 2020). While such indices can be beneficial for accurately extracting impervious surfaces in urban environments, (Kebede et al., 2022), the spectral signature of urban and built LULC presents challenges and confusion with other classes. As spectrally dark and light areas can be a source of confusion for some classifiers trying to extract built environments, we chose to minimize this issue and refine our classification accuracy by masking lava flows (Kolarik et al., 2023), and water/barren areas using existing NLCD products. Since NLCD data is not available annually, we used the 2013 NLCD to mask imagery for 2015, the 2016 NLCD for 2016, 2017, and 2018, the 2019 NLCD for 2019 and 2020, the 2021 NLCD for 2021 and 2022, and the latest 2023 NLCD for 2023 and 2024.

Table 2. Spectral Indices.

Index	Acronym	Band Calculation	Reference
Normalized Difference Vegetation Index	NDVI	$NDVI = \frac{NIR(B8) - RED(B4)}{NIR(B8) + RED(B4)}$	(Rouse et al., 1973)
Normalized Difference Built-Up Index	NDBI	$NDBI = \frac{SWIR(B11) - NIR(B8)}{SWIR(B11) + NIR(B8)}$	(Zha et al., 2003)
Built-Up Index	BUI	$BU = NDBI - NDVI$	(Kaimaris and Patias, 2016)

Urban Index	UI	$UI = \frac{SWIR(B12) - NIR(B8)}{SWIR(B12) + NIR(B8)}$	(Kawamura et al., 1996)
Normalized Built-up Area Index	NBAI	$NBAI = \frac{SWIR(B12) - (\frac{SWIR(B11)}{GREEN(B3)})}{SWIR(B12) + (\frac{SWIR(B11)}{GREEN(B3)})}$	(Waqar et al., 2012)
New Built-up Index	NBI	$NBI = \frac{RED(B4) \times SWIR(B12)}{NIR(B8)}$	(Jieli et al., 2010)
Road Index	RI	$RI = 1 - \frac{3 \times (B11, B8, B2)}{B8 + B11 + B2}$	(Ahmed et al., 2022; Reddy et al., 2019)
Bare Soil Index	BSI	$BSI = \frac{(RED(B4) + SWIR1(B11)) - (NIR(B8))}{(RED(B4) + SWIR1(B11)) + (NIR(B8))}$	(Rikimaru et al., 2002)

Sentinel-1 GRD products are delivered as analysis-ready through GEE, having been corrected radiometrically and topographically. Sentinel-1 imagery is advantageous for detecting built infrastructure as it is unimpeded by cloud cover and hence can provide continuous, timely monitoring due to its all-weather imaging capabilities (Koppel et al., 2017). Sentinel-1 transmits and receives reflected radio waves in either the vertical (V) or horizontal (H) polarizations, providing up to four bands at a 10 m spatial resolution in single polarization (VV and HH) and cross polarization (VH and HV). SAR accumulates backscattering signals from scenes and is structure sensitive, and therefore well-suited for built infrastructure detection as urban areas typically generate higher backscatter intensity (Koppel et al., 2017). Previously, backscatter characteristics and intensity have been used in building detection, estimating building height which is generally positively correlated with backscatter (Cho et al., 2023; Frantz et al., 2021; Koppel et al., 2017), and exploring building destruction post natural hazards, such as earthquakes (Cho et al., 2023; Pirrone et al., 2020). Using GEE, we acquired and filtered Sentinel-1 imagery. Sentinel-1 coverage across each year was highly varied with some years having very few images. To ensure Sentinel-1 representation across the SRP for each year, we included SAR imagery collected between March to September, rather than June to September, as some years, notably the earlier years (2015-2018) had very few Sentinel-1 images.

For our classes of interest representing the built infrastructure we determined which variables are most useful for each class through variable importance plots to ensure these would be used to train the classifier. We selected all high quality images within the growing season between June and September for every year and created a single composite image consisting of the median value for each pixel. The result was annual image stacks from 2015 to 2024 with masked, median Sentinel-2 and Sentinel-1 composites with 22 covariates, including spectral bands and derived indices. Slope and aspect were included as additional topographic variables from the USGS National Elevation Dataset (NED), as both are critical factors in determining the suitability and sustainability of built environments. After performing an initial classification, we chose to also include distance to water using HydroSHEDS Free Flowing Rivers Network, distance to roads and distance to railways using US Census Bureau TIGER/Line Shapefiles for each year to improve confusion areas between the residential and vegetation classes.

2.1.2 Classification

Of the supervised classification techniques, RF is more commonly used for LULC classification over other classifiers as it is highly efficient, accurate, and readily scalable (Tassi and Vizzari, 2020). A recent comparison of the performance of SVM, CART, and RF in GEE to map LULC using Sentinel-2 revealed that RF outperformed the other ML models

(Zhao et al., 2024). RF is a non-parametric ML approach that combines multiple decision trees, and is suited to multi-class outputs (Nguyen et al., 2020). Available as a classifier in GEE, RF has been used successfully in previous studies focused on urban and built environment classification (Di Shi and Yang, 2017; Phan et al., 2020), and land use mapping in semi-arid areas (Abida et al., 2022). In GEE we applied our 100-tree RF classifier to each raster stack and produced annual maps across the SRP spanning 2015 to 2024.

2.1.3 Accuracy Assessment and Validation

Rigorous accuracy assessments are an essential component of developing any LULC product (Radeloff et al., 2024; Zhang and Li, 2022; Zhang and Roy, 2017), and should adhere to best practices (Olofsson et al., 2014). With supervised image classification, it is important that the training and validation datasets originate from separate samples to avoid biased accuracy assessments (Narducci et al., 2019). To that end, we evaluated our classification output using independent validation data generated through an equal allocation stratified random sampling design. Comparative to a simple random sampling design, an equal allocation stratification increases sampling rates for classes of interests that may be more rare in the study region, and also ensures that each pixel with data has a non-zero selection probability (Olofsson et al., 2014; Stehman and Foody, 2019). We selected three years - 2016, 2020, and 2024 - for validation and to evaluate classifier performance as these years did not have associated training data. For each year, we randomly selected 100 pixels per class, resulting in a yearly sample size of 600, and a total sample size of 1800 across the three validation years. For each pixel, we created a reference label by visually inspecting the corresponding Sentinel-2 image composite for the validation year. Though instances were few, we addressed mixed pixel problems by visually comparing the Sentinel-2 composite to NAIP imagery and then labeling to the nearest identifiable pixel relative to the Sentinel-2 imagery.

To assess the accuracy of the RF classifier we used a confusion matrix. Confusion or error matrices provide the proportion of area that is correctly classified for each class and also the proportion of area that is incorrectly classified for each class (Stehman, 2014). From the confusion matrix, we present popular accuracy measures, including Overall Accuracy (OA), Producer's Accuracy (PA), User's Accuracy (UA), Omission error (OE) and Commission error (CE). To assess the accuracy of the RF classifier, we used area adjusted producer's accuracies (PA) to estimate the omission bias of the classifiers for a given class (sensitivity), and user's accuracies (UA) to estimate commission biases (specificity), as well as associate variance estimators to calculate 95% confidence intervals. To smooth the classified images, we removed small isolated regions consisting of two pixels or fewer of the same classification.

2.1.4 Time Series Analysis and Product Comparison

We used our mapped product to explore changes in built infrastructure over time across the SRP. We calculated area estimations for each class across the SRP to quantify how much change was observed over the time series. We isolated built infrastructure classes and explored area trends, spatial patterns and change across the SRP from 2015 to 2024.

We compared our SRP time series with three publicly available LULC products: NLCD, MBF and DW using area estimate comparison and visual spatial comparison. Our mapped products have three classes representing built infrastructure: residential, infrastructure and paved (Table 1). In terms of thematic resolution, MBF does not have classes. NLCD has four 'developed' classes representing the built infrastructure with varying intensity of impervious surfaces and DW has one: 'built' (Table 1). Our mapped products

have the same spatial resolution as DW: 10 m, which is a finer spatial resolution than the 30 m NLCD, but a coarser spatial resolution than MBF. MBF has the highest spatial resolution of all four products. Temporally, our mapped products are annual for the time series 2015 to 2024 which also matches DW (Figure 4). Both our mapped products and DW have a finer temporal resolution than both NLCD and MBF, with the caveat that MBF has temporal uncertainty with being trained on Bing maps for the years 2014 to 2020 (Figure 4).

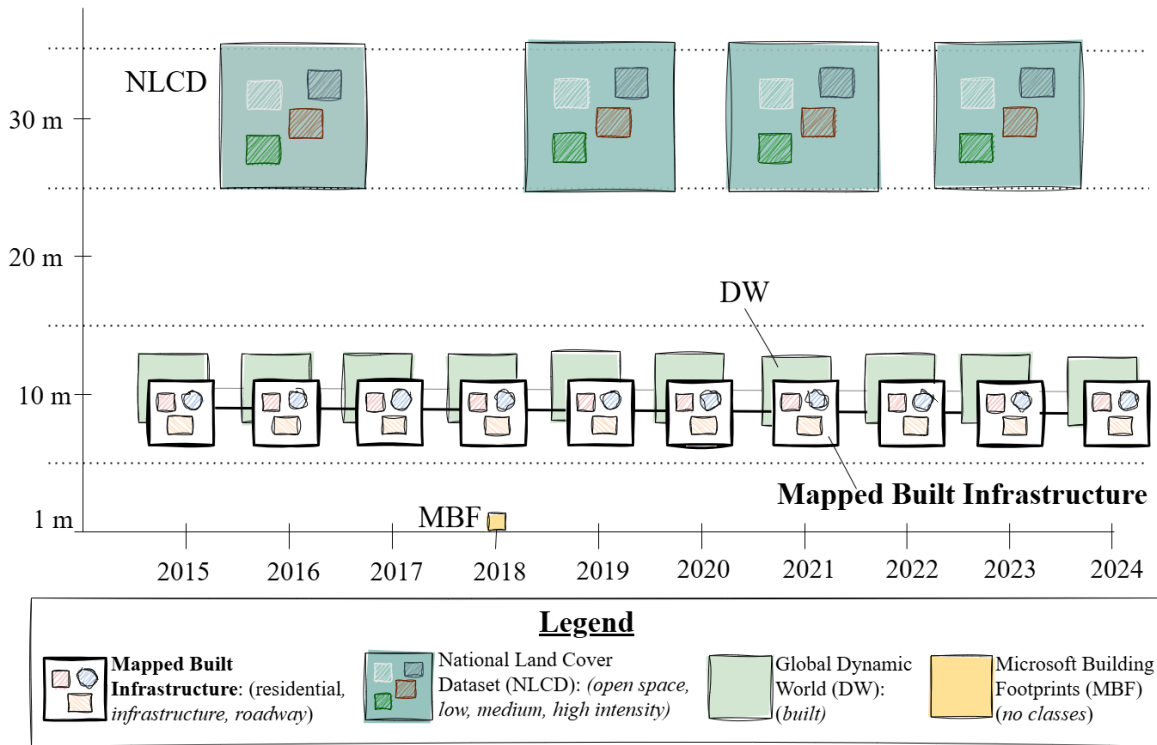


Figure 4. Comparing spatial, temporal and thematic resolutions of existing LULC products to our mapped built infrastructure (MBI) products. Both DW and MBI have a spatial resolution of 10 m and thus have an identical pixel size, but these products differ in their thematic resolution. The higher thematic resolution of MBI is illustrated by the three hatched shapes within the black square; however, these do not represent sub-pixel features, but rather serve as a schematic to demonstrate the enhanced thematic detail of our product, compared to the single ‘built’ class in DW. Likewise, the four hatched shapes within the NLCD represent the four ‘developed’ classes.

Using GEE, we processed existing LULC products before comparing them to our mapped products. We acquired NLCD for the available years: 2016, 2019, 2021, and 2023. We filtered DW by date to match our products, and created annual DW composites 2015 to 2024. We filtered and clipped both datasets using the SRP boundary. We calculated the annual area estimates in km² for each class representing the built environment in NLCD, DW and our mapped products and we explored the change in these classes over these different time series. We then compared area estimates and spatial distribution across these products to explore whether there was any correspondence. Using QGIS, we extracted a total of 625,997 building footprints across the SRP ecoregion from the MBF data. As the MBF does not have a time series, we calculated the area in km² of these footprints to get the total MBF coverage across the SRP.

3. Results and Discussion

3.1 Mapping Built Infrastructure

We applied our RF classifier to ten image stacks containing a fusion of Sentinel-2 and Sentinel-1 time series imagery and generated annual mapped products across the SRP for the time series 2015 to 2024. Our mapped product distinguished the six different classes well, with OAs of 90.5% ($\pm 7.5\%$) for 2016, 93.6% ($\pm 7.14\%$) for 2020, and 96.3% ($\pm 6.98\%$) for 2024. Of the built infrastructure classes, the PA was consistently highest for the infrastructure class ranging from 97.94% ($\pm 16.26\%$) to 99.70 ($\pm 2.95\%$), followed by the residential class with PAs ranging from 90.98% ($\pm 11.46\%$) to 96.42% ($\pm 3.35\%$). PAs were lowest for the paved class. The UAs were consistently higher for the paved class compared with the other infrastructure classes, followed by the residential class and then the infrastructure class. Area estimations of both residential and infrastructure classes increased over time from 2016 to 2024. Our product poorly captured the range/scrub class which had the lowest PA of 31.48% ($\pm 14.11\%$) in 2016, and a similarly low PA in 2024 of 31.53 ($\pm 16.09\%$). In addition, our product does not capture agriculture as well as built classes, with the lowest PA at 51.15% ($\pm 4.63\%$). The vegetation and range/scrub classes had the highest UAs, all above 99%, with the exception of the range/scrub class for the year 2020 which was 73.25% ($\pm 8.72\%$).

For our classifier, Distance to Railways was the most important variable for distinguishing the three built infrastructure classes: residential, infrastructure and paved, from the other classes, with a variable importance score of 6.85%. Distance to Roads and Distance to Rivers were also valuable for this model, with variable importance scores of 5.61% and 5.40%, respectively. Sentinel-1 variables, specifically VH and VV were also important for this model, more so than the derived spectral indices (5.05% and 4.57%, respectively). Of the spectral indices, RI was the most important (4.56%), followed by UI (4.03%), and NBAI (4.02%).

Across the SRP, we found that the residential class increased by 8.62% between 2016 (383 km²) and 2024 (416 km²), similarly the infrastructure class increased by 7.23% (318 km² to 341 km²) (Figure 5, Figure 6). Though built infrastructure change was heterogeneous across the SRP, exploring the time series at the ecoregion level reveals increases in all three built classes over time in our mapped product, a trend which is also reflected in the DW Built class and most NLCD classes (Figure 6).

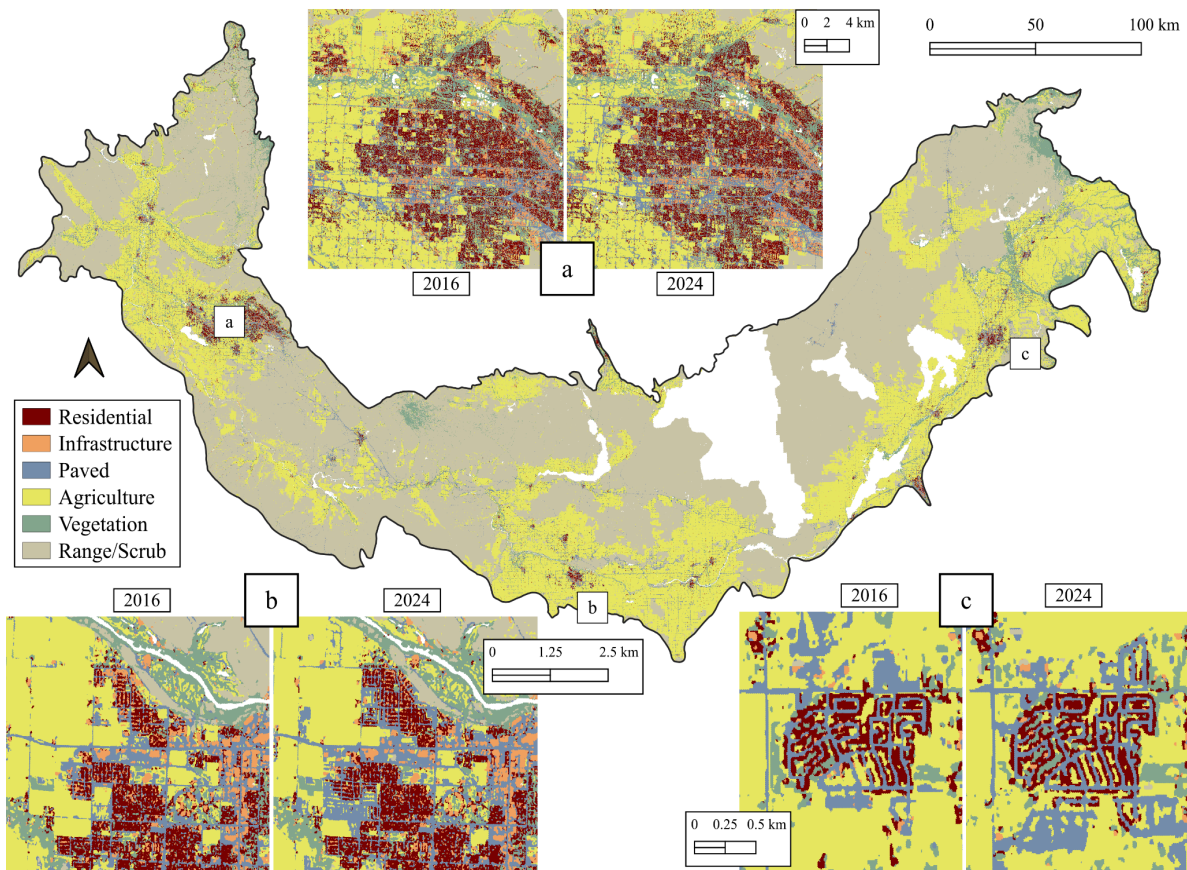


Figure 5. Classification results for the year 2024 across the Snake River Plain (SRP), and comparisons between 2016 and 2024 classifications in **(a)** Boise (west SRP), **(b)** suburbs to the north of Twin Falls (south SRP), and **(c)** Ammon, a suburb city to the east of Idaho Falls (east SRP).

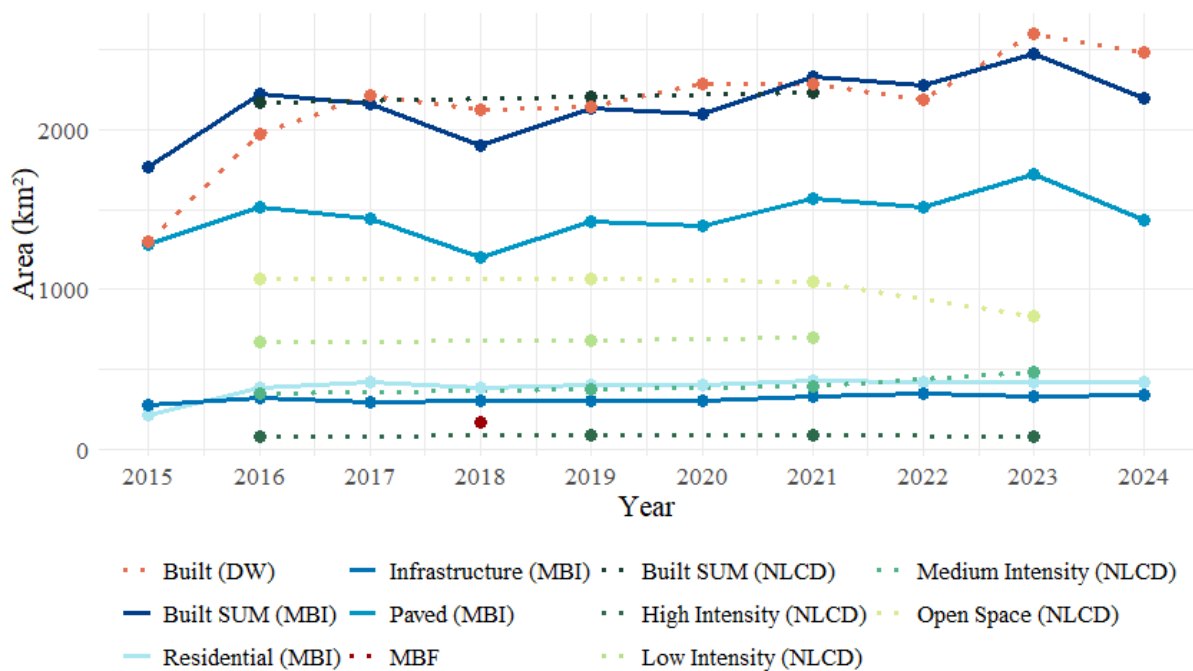
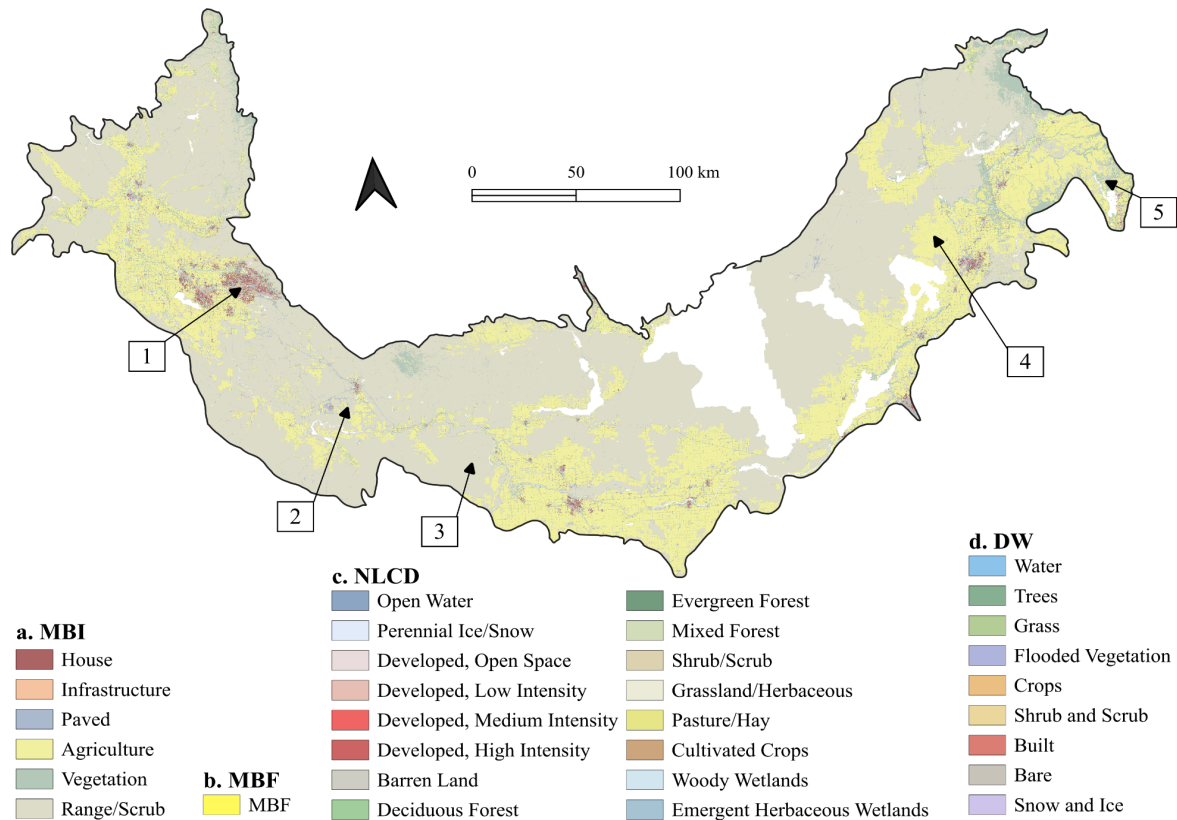


Figure 6. Comparing class areas (km²) across the SRP as mapped by different LULC products, including our mapped built infrastructure (MBI) product, global Dynamic World

(DW), Microsoft Building Footprints (MBF), and National Land Cover Dataset (NLCD). 2023 values for the NLCD Low Intensity class were surprisingly high, with a 161% increase in area for this particular class, from 697 km² in 2021 to 1816 km² in 2021. Released in October 2024, the 2023 NLCD data mostly compare well with previous years, however this increase seems questionable. As such, we have omitted the NLCD Low Intensity class and Built SUM for the year 2023.

From the NLCD products for 2016, 2019, and 2021 the total extent of the four developed classes across the SRP was as follows: 2,170 km², 2,208 km², and 2,228 km². For the same years, the extent of the DW Built class was: 1,972 km², 2,145 km² and 2,287 km², respectively. In comparison, the sum of our three built classes for the same years was: 2,219 km², 2,132 km², and 2,333 km². Overall, there is congruence between the total built area in our MBI product (MBI Built Sum), NLCD (NLCD Built Sum), and the DW Built class (Figure 8). Visually comparing specific classes reveals that the MBI Residential class is most similar to the NLCD Medium Intensity class. Comparing across the years that NLCD is available, 2016 to 2021, the NLCD classes with the most growth during this period were Medium and High Intensity, 12.30% and 9.20%, respectively. The Low Intensity class only increased by 3.44%, while the Open Space class decreased in area by 1.35%. During this same period, all the MBI classes experienced increases in area extent, with the MBI Residential class experiencing the most growth (13.10%), followed by Infrastructure (4.40%), and Paved (3.29%). MBI Built classes combined grew by 5.1% between 2016 and 2021, while the DW Built class increased in extent by 6.69%.

For the year 2024, our products estimate that 5.88% (3117 km²) of the SRP is classified as built-up land (residential, infrastructure and paved combined), compared to 6% estimated by the NLCD and 4.64% by DW. Visual comparisons of our classification compared to NLCD, DW and MBF are provided in Figure 7.



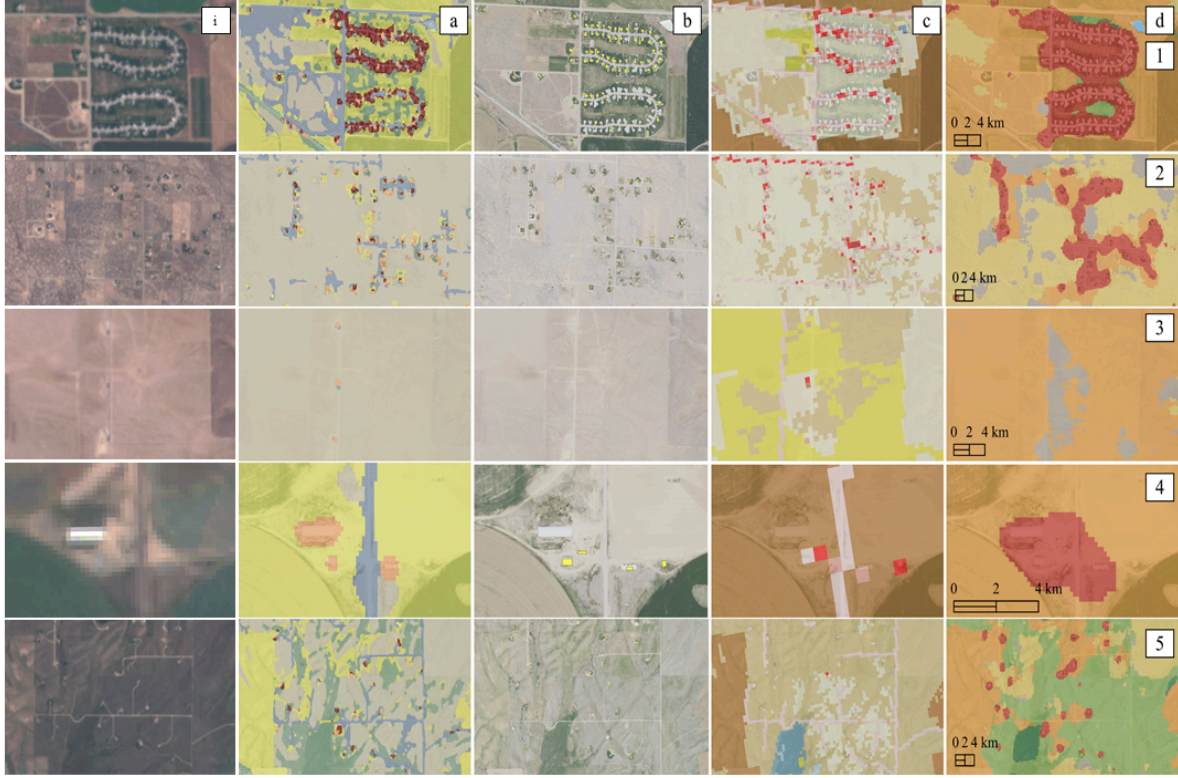


Figure 7. Spatial comparison of classes between (a) our mapped built infrastructure, (b) Microsoft Building Footprints (MBF) (c) National Land Cover Dataset (NLCD) and (d) Dynamic World (DW) for the year 2021.

Our mapped products offer advantages for capturing built infrastructure over current LULC products. Our time series improves on existing products in terms of spatial, temporal and thematic resolutions.

We found that the finer spatial and temporal resolution from the Sentinel fusion time series generate more accurate and detailed LULC maps compared to existing national pixel-based datasets produced solely from Landsat, and global pixel-based datasets produced solely from Sentinel-2. LULC classes in existing products are lacking detail for parsing out specific types of infrastructure accurately (Sleeter, 2012). Although NLCD has four built classes which is a thematic improvement on the global DW dataset, these classes are intensity-based. As such they do not allow for the identification and differentiation of residential properties, and single-family housing units commonly characterize three of these classes (Table 1). Like the DW dataset, our pixel-based product used Sentinel-2 but with the addition of Sentinel-1 SAR. Although the global DW is partially derived from the same imagery and has the same spatial resolution as our product, our time series has three built classes to the DW's one; and thus offers improvements for differentiating between types of urban development, particularly for identifying residential properties.

Created using deep learning and a polygonization algorithm for edge detection, the MBF has the highest spatial resolution of all existing products, including ours, however these data have some deficiencies. In alignment with previous reports (Carlson et al., 2022; Heris et al., 2020), building classification errors of commission and omission are present in the MBF dataset; we encountered errors of commission and omission. While MBF accurately captures most building footprints, these data do not allow for differentiation between building types, for example, separating homes from agricultural and resource extraction infrastructure.

The high OAs of our classifier and spectral separability of the built classes,

particularly Residential and Infrastructure, in our semi-arid system gives hope that built infrastructure types can also be differentiated in other systems. Rather than global or even national products (Wyborn and Evans, 2021), our product gives support for regionally parameterized models that can more accurately capture built infrastructure change over time. Our work demonstrates the opportunities that improvements in remote sensing technologies offer for parsing residential homes from other types of built infrastructure, and supports existing literature demonstrating that classifying built infrastructure using remote sensing imagery can produce mapped products of development and urban intensity that are superior to those found in NLCD (Abida et al., 2022). Creating accurate, timely LULC maps with improved thematic resolution to delineate where people are residing may be more helpful for informing policy and decision-making both within and outside the WUI, land use planning, food security assessments and natural hazard and disaster responses than existing products with single or intensity-based built classes.

4. Conclusions and Implications for Management/Policy and Future Research

4.1 Key Findings and Implications for Management/Policy

Accurate and timely built infrastructure maps have broad applicability and can be critically important for informing policy, decision-making, land use planning, food security assessments, natural hazard and disaster responses and evaluating conservation efforts. We employed a fusion of Sentinel products and generated annual maps of built infrastructure spanning 2015 to 2024 using a combination of open-source, freely available software, cloud computing, and imagery. Our time series improves on existing built infrastructure products in spatial, temporal and thematic resolution. Advances in remote sensing imagery, particularly increases in spatial resolution, offer promise for differentiating built infrastructure types and for detecting smaller features, such as low-density built infrastructure, that can improve upon existing LULC maps derived from more spatially coarse imagery. Image classification represents an opportunity to leverage open-source approaches and data, from using cloud computing and freely available remote sensing imagery, to generating products with accompanying detailed open-source workflows.

Delineating the areas where built infrastructure is close to wildland vegetation, described as the wildland-urban interface (WUI), is important for numerous human-environmental land management challenges beyond wildfire, including habitat loss, ecosystem fragmentation, declining biodiversity, invasive species spread, disease transfer, and land cover conversion. Wildfire is a critical concern in the WUI, as infrastructure expansion increases both fire ignitions and the number of residential properties at risk. While the WUI alone does not directly define fire risk, its delineation influences fire risk management. However, the use of WUI maps to guide wildfire risk decisions is not well understood. We reviewed various WUI definitions and conceptualizations in the context of wildfire risk management. WUI operationalizations should consider spatial scale: standardized WUI definitions hold value for large spatial-scale WUI mapping, ensuring consistency and comparability at national or global levels, while region-specific WUI definitions offer more flexibility to capture local conditions and variability. We emphasize that WUI maps were not designed to represent fire risk, and should not be relied upon as the sole tool for guiding wildfire risk management. Once WUI and non-WUI areas are delineated, these maps should be combined with additional data sources for a more accurate assessment of fire risk prior decision-making. This integration should leverage recent advancements in remote sensing, geospatial

technologies, and center local knowledge and community collaboration, to capture the key factors influencing fire risk both within and outside the WUI.

Ultimately, this research demonstrates the value of regionally parameterized LULC models and local-regional WUI maps to inform management and decision-making that is place-based and considers local conditions. We emphasize the importance of being able to identify residential versus other infrastructure types, and highlight that our MBI products have wide application, beyond WUI delineations.

4.2 Future Research

Open-source and freely available imagery and software enables a broader audience to use these workflows and products. We recommend that future research employ open-source and freely available imagery and software for reproducibility and transparency.

We identified future research needs which include, but are not limited to: as including:

- i) tailoring other LULC maps to other less studied systems
- ii) utilizing finer-scale remote sensing imagery, such as with spatial resolutions finer than 5 m, and considering combining lidar, to more accurately capture and parse between more built infrastructure types and vegetation. This could be especially relevant for built linear features, such as powerlines and fences.
- iii) producing mapped products at sub-annual resolution to track seasonal, monthly, or weekly change – such finer-temporally resolved maps would be particularly useful for natural hazard and disaster response, including mitigating human exposure to wildfire in both the WUI and non-WUI.

5. Literature Cited

Abida, K., Barbouchi, M., Boudabbous, K., Toukabri, W., Saad, K., Bousnina, H., Sahli Chahed, T., 2022. Sentinel-2 data for land Use mapping: comparing different supervised classifications in semi-arid areas. *Agriculture* 12, 1429.
<https://doi.org/10.3390/agriculture12091429>.

Ager, A.A., Evers, C.R., Day, M.A., Alcasena, F.J., Houtman, R., 2021. Planning for future fire: scenario analysis of an accelerated fuel reduction plan for the western United States. *Landsc. Urban Plan.* 215, 104212. <https://doi.org/10.1016/j.landurbplan.2021.104212>.

Ahmed, M.W., Saadi, S., Ahmed, M., 2022. Automated road extraction using reinforced road indices for Sentinel-2 data. *Array* 16, 100257.
<https://doi.org/10.1016/j.array.2022.100257>.

Ali, K., Johnson, B.A., 2022. Land-use and land-cover classification in semi-arid areas from medium-resolution remote-sensing imagery: a deep learning approach. *Sensors* 22, 8750.
<https://doi.org/10.3390/s22228750>.

Amani, M., Ghorbanian, A., Ahmadi, S.A., Kakooei, M., Moghimi, A., Mirmazloumi, S.M., Moghaddam, S.H.A., Mahdavi, S., Ghahremanloo, M., Parsian, S., Wu, Q., Brisco, B., 2020. Google earth engine cloud computing platform for remote sensing big data applications: a comprehensive review. *IEEE J. Sel. Top. Appl. Earth Obs. Remote Sens.* 13, 5326–5350.
<https://doi.org/10.1109/JSTARS.2020.3021052>.

Bartsch, A., Pointner, G., Ingeman-Nielsen, T., Lu, W., 2020. Towards circumpolar mapping of arctic settlements and infrastructure based on sentinel-1 and sentinel-2. *Remote Sens* 12, 2368. <https://doi.org/10.3390/rs12152368>.

Brown, C.F., Brumby, S.P., Guzder-Williams, B., Birch, T., Hyde, S.B., Mazzariello, J., Czerwinski, W., Pasquarella, V.J., Haertel, R., Ilyushchenko, S., Schwehr, K., Weisse, M., Stolle, F., Hanson, C., Guinan, O., Moore, R., Tait, A.M., 2022. Dynamic World, Near real-time global 10 m land use land cover mapping. *Sci. Data* 9, 251. <https://doi.org/10.1038/s41597-022-01307-4>.

Campbell, J.B., Wynne, R.H., 2011. *Introduction to Remote Sensing*, fifth ed. Guilford Publications, New York, United States.

Carlson, A.R., Helmers, D.P., Hawbaker, T.J., Mockrin, M.H., Radeloff, V.C., 2022. The wildland–urban interface in the United States based on 125 million building locations. *Ecol. Appl.* 32, e2597. <https://doi.org/10.1002/eap.2597>.

Chaves M, E.D., Picoli M, C.A., Sanches, I.D., 2020. Recent applications of Landsat 8/OLI and sentinel-2/MSI for land use and land cover mapping: a systematic review. *Remote Sens* 12, 3062. <https://doi.org/10.3390/rs12183062>.

Chen, Jun, Chen, Jin, Liao, A., Cao, X., Chen, L., Chen, X., He, C., Han, G., Peng, S., Lu, M., Zhang, W., Tong, X., Mills, J., 2015. Global land cover mapping at 30m resolution: a POK-based operational approach. *ISPRS J. Photogramm. Remote Sens.* 103, 7–27. <https://doi.org/10.1016/j.isprsjprs.2014.09.002>.

Chen, T.-H.K., Qiu, C., Schmitt, M., Zhu, X.X., Sabel, C.E., Prishchepov, A.V., 2020. Mapping horizontal and vertical urban densification in Denmark with Landsat time-series from 1985 to 2018: a semantic segmentation solution. *Remote Sens. Environ.* 251, 112096. <https://doi.org/10.1016/j.rse.2020.112096>.

Cho, S., Xiu, H., Matsuoka, M., 2023. Backscattering characteristics of SAR images in damaged buildings due to the 2016 kumamoto earthquake. *Remote Sens* 15, 2181. <https://doi.org/10.3390/rs15082181>.

Dagne, S.S., Hirpha, H.H., Tekoye, A.T., Dessie, Y.B., Endeshaw, A.A., 2023. Fusion of sentinel-1 SAR and sentinel-2 MSI data for accurate Urban land use-land cover classification in Gondar City, Ethiopia. *Environ. Syst. Res.* 12, 40. <https://doi.org/10.1186/s40068-023-00324-5>.

Dahal, K.R., Benner, S., Lindquist, E., 2018. Analyzing spatiotemporal patterns of urbanization in Treasure Valley, Idaho, USA. *Appl. Spat. Anal. Policy* 11, 205–226. <https://doi.org/10.1007/s12061-016-9215-1>.

De Fioravante, P., Luti, T., Cavalli, A., Giuliani, C., Dichicco, P., Marchetti, M., Chirici, G., Congedo, L., Munafo, M., 2021. Multispectral sentinel-2 and SAR sentinel-1 integration for automatic land cover classification. *Land* 10, 611. <https://doi.org/10.3390/land10060611>.

De Luca, G., Silva J, M.N., Di Fazio, S., Modica, G., 2022. Integrated use of Sentinel-1 and

Sentinel-2 data and open-source machine learning algorithms for land cover mapping in a Mediterranean region. *Eur. J. Remote Sens.* 55, 52–70.
<https://doi.org/10.1080/22797254.2021.2018667>.

DeVries, B., Huang, C., Armston, J., Huang, W., Jones, J.W., Lang, M.W., 2020. Rapid and robust monitoring of flood events using Sentinel-1 and Landsat data on the Google Earth Engine. *Remote Sens. Environ.* 240, 111664. <https://doi.org/10.1016/j.rse.2020.111664>.

Di Shi, Yang, X., 2017. A relative evaluation of random forests for land cover mapping in an urban area. *Photogramm. Eng. Rem. Sens.* 83, 541–552.
<https://doi.org/10.14358/PERS.83.8.541>.

Digra, M., Dhir, R., Sharma, N., 2022. Land use land cover classification of remote sensing images based on the deep learning approaches: a statistical analysis and review. *Arab. J. Geosci.* 15, 1003. <https://doi.org/10.1007/s12517-022-10246-8>.

Farhan, M., Wu, T., Amin, M., Tariq, A., Guluzade, R., Alzahrani, H., 2024. Monitoring and prediction of the LULC change dynamics using time series remote sensing data with Google Earth Engine. *Phys. Chem. Earth, Parts A/B/C* 136, 103689.
<https://doi.org/10.1016/j.pce.2024.103689>.

Frantz, D., Schug, F., Okujeni, A., Navacchi, C., Wagner, W., van der Linden, S., Hostert, P., 2021. National-scale mapping of building height using Sentinel-1 and Sentinel-2 time series. *Remote Sens. Environ.* 252, 112128. <https://doi.org/10.1016/j.rse.2020.112128>.

Friedl, M.A., Woodcock, C.E., Olofsson, P., Zhu, Z., Loveland, T., Stanimirova, R., Arevalo, P., Bullock, E., Hu, K.-T., Zhang, Y., Turlej, K., Tarrio, K., McAvoy, K., Gorelick, N., Wang, J.A., Barber, C.P., Souza, C., 2022. Medium spatial resolution mapping of global land cover and land cover change across multiple decades from Landsat. *Front. Remote Sens.* 3.
<https://doi.org/10.3389/frsen.2022.894571>.

Ganjirad, M., Bagheri, H., 2024. Google Earth Engine-based mapping of land use and land cover for weather forecast models using Landsat 8 imagery. *Ecol. Inform.* 80, 102498. <https://doi.org/10.1016/j.ecoinf.2024.102498>.

Gargiulo, M., Dell’Aglia, D.A.G., Iodice, A., Riccio, D., Ruella, G., 2020. Integration of sentinel-1 and sentinel-2 data for land cover mapping using W-net. *Sensors* 20, 2969.
<https://doi.org/10.3390/s20102969>.

Ghanbari, M., Arabi, M., Georgescu, M., Broadbent, A.M., 2023. The role of climate change and urban development on compound dry-hot extremes across US cities. *Nat. Commun.* 14, 3509. <https://doi.org/10.1038/s41467-023-39205-x>.

Goldblatt, R., You, W., Hanson, G., Khandelwal, A.K., 2016. Detecting the boundaries of urban areas in India: a dataset for pixel-based image classification in google earth engine. *Remote Sens* 8, 634. <https://doi.org/10.3390/rs8080634>.

Goldblatt, R., Stuhlmacher, M.F., Tellman, B., Clinton, N., Hanson, G., Georgescu, M., Wang, C., Serrano-Candela, F., Khandelwal, A.K., Cheng, W.-H., Balling, R.C., 2018. Using Landsat and nighttime lights for supervised pixel-based image classification of urban land

cover. *Remote Sens. Environ.* 205, 253–275. <https://doi.org/10.1016/j.rse.2017.11.026>.

Gong, P., Li, X., Wang, J., Bai, Y., Chen, B., Hu, T., Liu, X., Xu, B., Yang, J., Zhang, W., Zhou, Y., 2020. Annual maps of global artificial impervious area (GAIA) between 1985 and 2018. *Remote Sens. Environ.* 236, 111510. <https://doi.org/10.1016/j.rse.2019.111510>.

Gorelick, N., Hancher, M., Dixon, M., Ilyushchenko, S., Thau, D., Moore, R., 2017. Google earth engine: planetary-scale geospatial analysis for everyone. *Remote Sens. Environ., Big Remotely Sensed Data: tools, applications and experiences* 202, 18–27. <https://doi.org/10.1016/j.rse.2017.06.031>.

Halperin, S., Castro, A.J., Quintas-Soriano, C., Brandt, J.S., 2023. Assessing high quality agricultural lands through the ecosystem services lens: insights from a rapidly urbanizing agricultural region in the western United States. *Agric. Ecosyst. Environ.* 349, 108435.

Handwerger, A.L., Huang, M.-H., Jones, S.Y., Amatya, P., Kerner, H.R., Kirschbaum, D.B., 2022. Generating landslide density heatmaps for rapid detection using open access satellite radar data in Google Earth Engine. *Nat. Hazards Earth Syst. Sci.* 22. <https://doi.org/10.5194/nhess-22-753-2022>.

Heris, M.P., Foks, N.L., Bagstad, K.J., Troy, A., Ancona, Z.H., 2020. A rasterized building footprint dataset for the United States. *Sci. Data* 7, 207. <https://doi.org/10.1038/s41597-020-0542-3>.

Homer, C.G., Xian, G., Aldridge, C.L., Meyer, D.K., Loveland, T.R., O'Donnell, M.S., 2015. Forecasting sagebrush ecosystem components and greater sage-grouse habitat for 2050: learning from past climate patterns and Landsat imagery to predict the future. *Ecol. Indic.* 55, 131–145. <https://doi.org/10.1016/j.ecolind.2015.03.002>.

Homer, C., Dewitz, J., Jin, S., Xian, G., Costello, C., Danielson, P., Gass, L., Funk, M., Wickham, J., Stehman, S., Auch, R., Riitters, K., 2020. Conterminous United States land cover change patterns 2001–2016 from the 2016 national land cover Database. *ISPRS J. Photogramm. Remote Sens.* 162, 184–199. <https://doi.org/10.1016/j.isprsjprs.2020.02.019>.

Huang, C., Xu, N., 2022. Quantifying urban expansion from 1985 to 2018 in large cities worldwide. *Geocarto Int.* 37, 18356–18371. <https://doi.org/10.1080/10106049.2022.2142957>.

Javed, A., Cheng, Q., Peng, H., Altan, O., Li, Y., Ara, I., Huq, MdE., Ali, Y., Saleem, N., 2021. Review of spectral indices for urban remote sensing. *Photogramm. Eng. Remote Sens.* 87, 513–524. <https://doi.org/10.14358/PERS.87.7.513>.

Jieli, C., Manchun, L., Yongxue, L., Chenglei, S., Wei, H., 2010. Extract residential areas automatically by new built-up index. 2010 18th Int. Conf. Geoinformatics 1–5. <https://doi.org/10.1109/GEOINFORMATICS.2010.5567823>.

Jochems, L.W., Brandt, J., Monks, A., Cattau, M., Kolarik, N., Tallant, J., Lishawa, S., 2021. Comparison of different analytical strategies for classifying invasive wetland vegetation in imagery from unpiloted aerial systems (UAS). *Remote Sens* 13, 4733. <https://doi.org/10.3390/rs13234733>.

Jones, K., Abrams, J., Belote, R.T., Beltr'an, B.J., Brandt, J., Carter, N., Castro, A.J., Chaffin, B.C., Metcalf, A.L., Roesch-McNally, G., Wallen, K.E., Williamson, M.A., 2019. The American West as a social-ecological region: drivers, dynamics and implications for nested social-ecological systems. *Environ. Res. Lett.* 14, 115008. <https://doi.org/10.1088/1748-9326/ab4562>.

Kaimaris, D., Patias, P., 2016. Identification and area measurement of the built-up area with the built-up index (BUI). *Int. J. Adv. Remote Sens. GIS* 5, 1844–1858. <https://doi.org/10.23953/cloud.ijarsg.64>.

Karimi, F., Sultana, S., 2024. Urban expansion prediction and land use/land cover change modeling for sustainable urban development. *Sustainability* 16, 2285. <https://doi.org/10.3390/su16062285>.

Kawamura, M., Jayamanna, S., Tsujiko, Y., 1996. Relation between social and environmental condition in colombo, Sri Lanka and the urban index estimated by satellite remote sensing data. *Int. Arch. Photogramm. Remote Sens.* 31, 321–326.

Kebede, T.A., Hailu, B.T., Suryabhagavan, K.V., 2022. Evaluation of spectral built-up indices for impervious surface extraction using Sentinel-2A MSI imageries: a case of Addis Ababa city, Ethiopia. *Environ. Chall.* 8, 100568. <https://doi.org/10.1016/j.envc.2022.100568>.

Ketchpaw, A.R., Li, D., Khan, S.N., Jiang, Y., Li, Y., Zhang, L., 2022. Using structure location data to map the wildland–urban interface in Montana, USA. *Fire* 5, 129. <https://doi.org/10.3390/fire5050129>.

Khan, A., Govil, H., Kumar, G., Dave, R., 2020. Synergistic use of Sentinel-1 and Sentinel-2 for improved LULC mapping with special reference to bad land class: a case study for Yamuna River floodplain, India. *Spat. Inf. Res.* 28, 669–681. <https://doi.org/10.1007/s41324-020-00325-x>.

Kolarik, N.E., Roopsind, A., Pickens, A., Brandt, J.S., 2023. A satellite-based monitoring system for quantifying surface water and mesic vegetation dynamics in a semiarid region. *Ecol. Indic.* 147, 109965. <https://doi.org/10.1016/j.ecolind.2023.109965>.

Koley, S., Chockalingam, J., 2022. Sentinel 1 and Sentinel 2 for cropland mapping with special emphasis on the usability of textural and vegetation indices. *Adv. Space Res., Advances in Spaceborne SAR Remote Sensing for Characterization of Natural and Manmade Features - Part 1* (69), 1768–1785. <https://doi.org/10.1016/j.asr.2021.10.020>.

Koppel, K., Zalite, K., Voormansik, K., Jagdhuber, T., 2017. Sensitivity of Sentinel-1 backscatter to characteristics of buildings. *Int. J. Remote Sens.* 38, 6298–6318.

Li, K., Wang, J., Cheng, W., Wang, Y., Zhou, Y., Altansukh, O., 2022. Deep learning empowers the google earth engine for automated water extraction in the lake baikal basin. *Int. J. Appl. Earth Obs. Geoinformation* 112, 102928. <https://doi.org/10.1016/j.jag.2022.102928>.

Li, S., Dao, V., Kumar, M., Nguyen, P., Banerjee, T., 2022. Mapping the wildland-urban

interface in California using remote sensing data. *Sci. Rep.* 12, 5789.

<https://doi.org/10.1038/s41598-022-09707-7>.

Liu, X., Hu, G., Chen, Y., Li, X., Xu, X., Li, S., Pei, F., Wang, S., 2018. High-resolution multi-temporal mapping of global urban land using Landsat images based on the Google Earth Engine Platform. *Remote Sens. Environ.* 209, 227–239.

<https://doi.org/10.1016/j.rse.2018.02.055>.

Lynch, P., Blesius, L., Hines, E., 2020. Classification of urban area using multispectral indices for urban planning. *Remote Sens* 12, 2503. <https://doi.org/10.3390/rs12152503>.

Mahler, R.L., 2019. The impact of agriculture on the waters of the Idaho portion of the Snake River Basin, USA. *Int. J. Sustain. Dev. Plan.* 14, 93–104.

<https://doi.org/10.2495/SDP-V14-N2-93-104>.

Mahler, R.L., 2020. The water nexus in southwestern Idaho, USA: development versus agriculture. *Int. J. Environ. Impacts Manag. Mitig. Recovery* 3, 248–259.

<https://doi.org/10.2495/EI-V3-N3-248-259>.

McRoberts, R.E., Liknes, G.C., Walters, B.F., 2018. The effects of imperfect reference data on remote sensing-assisted estimators of land cover class proportions. *ISPRS J. Photogramm. Remote Sens.* 142, 292–300.

<https://doi.org/10.1016/j.isprsjprs.2018.06.002>.

Monsalve-Tellez, J.M., Torres-Leon, J.L., Garc es-Gomez, Y.A., 2022. Evaluation of SAR and optical image fusion methods in oil palm crop cover classification using the random forest algorithm. *Agriculture* 12, 955. <https://doi.org/10.3390/agriculture12070955>.

Narducci, J., Quintas-Soriano, C., Castro, A.J., Som Castellano, R., Brandt, J., 2019. Implications of urban growth and farmland loss for ecosystem services in the western United States. *Land Use Pol.* 86, 1–11. <https://doi.org/10.1016/j.landusepol.2019.04.029>.

National Land Cover Database Class Legend and Description | Multi-Resolution Land Characteristics (MRLC) Consortium
<https://www.mrlc.gov/data/legends/national-land-cover-database-class-legend-and-description> (accessed [WWW Document], n.d. URL 7.30.24).

Netherton-Morrison, H., Hopping, K., Burnham, M., Som Castellano, R., Williamson, M., Wulforst, J.D., 2023. Statewide survey of Idahoan’s opinions on sagebrush landscapes, rangelands, and public lands. <https://doi.org/10.7923/1PBW-5718>.

Nguyen, L.H., Joshi, D.R., Clay, D.E., Henebry, G.M., 2020. Characterizing land cover/land use from multiple years of Landsat and MODIS time series: a novel approach using land surface phenology modeling and random forest classifier. *Remote Sens. Environ., Time Series Analysis with High Spatial Resolution Imagery*, 238, 111017.

<https://doi.org/10.1016/j.rse.2018.12.016>.

Olofsson, P., Foody, G., Herold, M., Stehman, S., Woodcock, C., Wulder, M., 2014. Good practices for assessing accuracy and estimating area of land change. *Remote Sens. Environ.* 148, 42–57. <https://doi.org/10.1016/j.rse.2014.02.015>.

Omernik, J.M., Griffith, G.E., 2014. Ecoregions of the conterminous United States: evolution of a hierarchical spatial framework. *Environ. Manage.* 54, 1249–1266. <https://doi.org/10.1007/s00267-014-0364-1>.

Parente, L., Taquary, E., Silva, A.P., Souza, C., Ferreira, L., 2019. Next generation mapping: combining deep learning, cloud computing, and big remote sensing data. *Remote Sens* 11, 2881. <https://doi.org/10.3390/rs11232881>.

Patel, N.N., Angiuli, E., Gamba, P., Gaughan, A., Lisini, G., Stevens, F.R., Tatem, A.J., Trianni, G., 2015. Multitemporal settlement and population mapping from Landsat using google earth engine. *Int. J. Appl. Earth Obs. Geoinformation* 35, 199–208. <https://doi.org/10.1016/j.jag.2014.09.005>.

Pérez-Cutillas, P., Pérez-Navarro, A., Conesa-García, C., Zema, D.A., Amado-Alvarez, J.P., 2023. What is going on within google earth engine? A systematic review and meta-analysis. *Remote Sens. Appl. Soc. Environ.* 29, 100907. <https://doi.org/10.1016/j.rsase.2022.100907>.

Pesaresi, M., Corbane, C., Julea, A., Florczyk, A.J., Syrris, V., Soille, P., 2016. Assessment of the added-value of sentinel-2 for detecting built-up areas. *Remote Sens* 8, 299. <https://doi.org/10.3390/rs8040299>.

Phan, T.N., Kuch, V., Lehnert, L.W., 2020. Land cover classification using google earth engine and random forest classifier—the role of image composition. *Remote Sens* 12, 2411. <https://doi.org/10.3390/rs12152411>.

Pirrone, D., Bovolo, F., Bruzzone, L., 2020. An approach to unsupervised detection of fully and partially destroyed buildings in multitemporal VHR SAR images. *IEEE J. Sel. Top. Appl. Earth Obs. Remote Sens.* 13, 5938–5953. <https://doi.org/10.1109/JSTARS.2020.3026838>.

Posit team, 2023. RStudio: integrated development environment for R. Posit Software.

QGIS.org, 2024. QGIS Geographic Information System.

Radeloff, V., Roy, D., Wulder, M., Anderson, M., Cook, B., Crawford, C., Friedl, M., Gao, F., Gorelick, N., Hansen, M., Healey, S., Hostert, P., Hulley, G., Huntington, J., Johnson, D., Neigh, C., Lyapustin, A., Lymburner, L., Pahlevan, N., Zhu, Z., 2024. Need and vision for global medium-resolution Landsat and Sentinel-2 data products. *Remote Sens. Environ.* 300, 113918. <https://doi.org/10.1016/j.rse.2023.113918>.

Reddy, S.L.K., Rao, C.V., Kumar, P.R., Anjaneyulu, R.V.G., Bothale, V.M., 2019. Automatic road feature extraction using MRF from LANDSAT-8 OLI images. In: 2019 IEEE Recent Advances in Geoscience and Remote Sensing : Technologies, Standards and Applications (TENGARSS). Presented at the 2019 IEEE Recent Advances in Geoscience and Remote Sensing : Technologies, Standards and Applications (TENGARSS), pp. 15–20. <https://doi.org/10.1109/TENGARSS48957.2019.8976046>.

Ren, Q., He, C., Huang, Q., Shi, P., Zhang, D., Güneralp, B., 2022. Impacts of urban expansion on natural habitats in global drylands. *Nat. Sustain.* 5, 869–878.

doi.org/10.1038/s41893-022-00930-8.

Requena-Mullor, J.M., Brandt, J., Williamson, M.A., Caughlin, T.T., 2023. Human population growth and accessibility from cities shape rangeland condition in the American West. *Landsc. Urban Plan.* 232, 104673.

Rigge, M., Homer, C., Cleeves, L., Meyer, D.K., Bunde, B., Shi, H., Xian, G., Schell, S., Bobo, M., 2020. Quantifying western U.S. Rangelands as fractional components with multi-resolution remote sensing and in situ data. *Remote Sens* 12, 412. <https://doi.org/10.3390/rs12030412>.

Rikimaru, A., Roy, P.S., Miyatake, S., 2002. Tropical forest cover density mapping. *Int. Soc. Trop. Ecol* 39–47.

Rouse, J., Haas, R.H., Schell, J.A., Deering, D., 1973. Monitoring Vegetation Systems in the Great Plains with ERTS.

Saah, D., Tenneson, K., Matin, M., Uddin, K., Cutter, P., Poortinga, A., Nguyen, Q.H., Patterson, M., Johnson, G., Markert, K., Flores, A., Anderson, E., Weigel, A., Ellenberg, W.L., Bhargava, R., Aekakkararungroj, A., Bhandari, B., Khanal, N., Housman, I.W., Potapov, P., Tyukavina, A., Maus, P., Ganz, D., Clinton, N., Chishtie, F., 2019. Land cover mapping in data scarce environments: challenges and opportunities. *Front. Environ. Sci.* 7.

Segarra, J., Buchailot, M.L., Araus, J.L., Kefauver, S.C., 2020. Remote sensing for precision agriculture: sentinel-2 improved features and applications. *Agronomy* 10, 641. <https://doi.org/10.3390/agronomy10050641>.

Seydi, S.T., Akhoondzadeh, M., Amani, M., Mahdavi, S., 2021. Wildfire damage assessment over Australia using sentinel-2 imagery and MODIS land cover product within the google earth engine cloud platform. *Remote Sens* 13, 220. <https://doi.org/10.3390/rs13020220>.

Singha, M., Dong, J., Sarmah, S., You, N., Zhou, Y., Zhang, G., Doughty, R., Xiao, X., 2020. Identifying floods and flood-affected paddy rice fields in Bangladesh based on Sentinel-1 imagery and Google Earth Engine. *ISPRS J. Photogramm. Remote Sens.* 166, 278–293. <https://doi.org/10.1016/j.isprsjprs.2020.06.011>.

Sleeter, B.M., 2012. Chapter 24 Snake River Plain ecoregion. In: *Status and Trends of Land Change in the Western United States—1973 to 2000*. U.S. Geological Survey Professional Paper 1794-A, pp. 246–253.

Stehman, S.V., 2014. Estimating area and map accuracy for stratified random sampling when the strata are different from the map classes. *Int. J. Rem. Sensing* 35 (13), 4923–4939. <https://doi.org/10.1080/01431161.2014.930207>.

Stehman, S.V., Foody, G.M., 2019. Key issues in rigorous accuracy assessment of land cover products. *Remote Sens. Environ.* 231, 111199. <https://doi.org/10.1016/j.rse.2019.05.018>.

Steinhausen, M.J., Wagner, P.D., Narasimhan, B., Waske, B., 2018. Combining Sentinel-1

and Sentinel-2 data for improved land use and land cover mapping of monsoon regions. *Int. J. Appl. Earth Obs. Geoinformation* 73, 595–604. <https://doi.org/10.1016/j.jag.2018.08.011>.

Szantoi, Z., Geller, G.N., Tsendbazar, N.-E., See, L., Griffiths, P., Fritz, S., Gong, P., Herold, M., Mora, B., Obregon, A., 2020. Addressing the need for improved land cover map products for policy support. *Environ. Sci. Policy* 112, 28–35. <https://doi.org/10.1016/j.envsci.2020.04.005>.

Tassi, A., Vizzari, M., 2020. Object-oriented LULC classification in google earth engine combining SNIC, GLCM, and machine learning algorithms. *Remote Sens* 12, 3776. <https://doi.org/10.3390/rs12223776>.

Velastegui-Montoya, A., Montalvan-Burbano, N., Carrion-Mero, P., Rivera-Torres, H., Sadeck, L., Adami, M., 2023. Google earth engine: a global analysis and future trends. *Remote Sens* 15, 3675. <https://doi.org/10.3390/rs15143675>.

Venkatappa, M., Sasaki, N., Han, P., Abe, I., 2021. Impacts of droughts and floods on croplands and crop production in Southeast Asia – an application of Google Earth Engine. *Sci. Total Environ.* 795, 148829. <https://doi.org/10.1016/j.scitotenv.2021.148829>.

Wang, P., Wang, J., Chen, Y., Ni, G., 2013. Rapid processing of remote sensing images based on cloud computing. *Future Gener. Comput. Syst., Including Special sections: Advanced Cloud Monitoring Systems & The fourth IEEE International Conference on e-Science 2011 — e-Science Applications and Tools & Cluster, Grid, and Cloud Computing* 29, 1963–1968. <https://doi.org/10.1016/j.future.2013.05.002>.

Waqar, M.M., Mirza, J.F., Mumtaz, R., Hussain, E., 2012. Development of New Indices for Extraction of Built-Up Area & Bare Soil from Landsat Data 1.

Whisenant, S.G., 1989. Changing fire frequencies on Idaho's Snake River plains: ecological and management implications. In: *Proceedings of a Symposium on Cheatgrass Invasion, Shrub Die-Off, and Other Aspects of Shrub Biology and Management*, pp. 4–10.

White, E.V., Roy, D.P., 2015. A contemporary decennial examination of changing agricultural field sizes using Landsat time series data. *Geo Geogr. Environ.* 2 (4), 33–54. <https://doi.org/10.1002/geo2>.

Wickham, H., Averick, M., Bryan, J., Chang, W., McGowan, L.D., François, R., Grolemund, G., Hayes, A., Henry, L., Hester, J., Kuhn, M., Pedersen, T.L., Miller, E., Bache, S.M., Müller, K., Ooms, J., Robinson, D., Seidel, D.P., Spinu, V., Takahashi, K., Vaughan, D., Wilke, C., Woo, K., Yutani, H., 2019. Welcome to the tidyverse. *J. Open Source Softw.* 4, 1686. <https://doi.org/10.21105/joss.01686>.

Wickham, J., Stehman, S.V., Sorenson, D.G., Gass, L., Dewitz, J.A., 2021. Thematic accuracy assessment of the NLCD 2016 land cover for the conterminous United States. *Remote Sens. Environ.* 257, 112357. <https://doi.org/10.1016/j.rse.2021.112357>.

Wickham, H., François, R., Henry, L., Müller, K., Vaughan, D., RStudio, 2023. *Dplyr: A Grammar of Data Manipulation*.

Wilkinson, M.D., Dumontier, M., Aalbersberg, I.J., Appleton, G., Axton, M., Baak, A., Blomberg, N., Boiten, J.-W., da Silva Santos, L.B., Bourne, P.E., Bouwman, J., Brookes, A.J., Clark, T., Crosas, M., Dillo, I., Dumon, O., Edmunds, S., Evelo, C.T., Finkers, R., Gonzalez-Beltran, A., Gray, A.J.G., Groth, P., Goble, C., Grethe, J.S., Heringa, J., t Hoen, P.A.C., Hooft, R., Kuhn, T., Kok, R., Kok, J., Lusher, S.J., Martone, M.E., Mons, A., Packer, A.L., Persson, B., Rocca-Serra, P., Roos, M., van Schaik, R., Sansone, S.-A., Schultes, E., Sengstag, T., Slater, T., Strawn, G., Swertz, M.A., Thompson, M., van der Lei, J., van Mulligen, E., Velterop, J., Waagmeester, A., Wittenburg, P., Wolstencroft, K., Zhao, J., Mons, B., 2016. The FAIR Guiding Principles for scientific data management and stewardship. *Sci. Data* 3, 160018. <https://doi.org/10.1038/sdata.2016.18>.

Wyborn, C., Evans, M.C., 2021. Conservation needs to break free from global priority mapping. *Nat. Ecol. Evol.* 5, 1322–1324. <https://doi.org/10.1038/s41559-021-01540-x>.

Xie, Y., Hunter, M., Sorensen, A., Nogueira-McRae, T., Murphy, R., Suraci, J.P., Lischka, S., Lark, T.J., 2023. U.S. Farmland under threat of urbanization: future development scenarios to 2040. *Land* 12, 574. <https://doi.org/10.3390/land12030574>.

Xu, C., Du, X., Fan, X., Giuliani, G., Hu, Z., Wang, W., Liu, J., Wang, T., Yan, Z., Zhu, J., Jiang, T., Guo, H., 2022. Cloud-based storage and computing for remote sensing big data: a technical review. *Int. J. Digit. Earth* 15, 1417–1445. <https://doi.org/10.1080/17538947.2022.2115567>.

Yang, X., Chen, Y., Wang, J., 2020. Combined use of Sentinel-2 and Landsat 8 to monitor water surface area dynamics using Google Earth Engine. *Remote Sens. Lett* 11, 687–696. <https://doi.org/10.1080/2150704X.2020.1757780>.

Yin, F., 2024. MarcYin/SIAC_GEE.

Zha, Y., Gao, J., Ni, S., 2003. Use of normalized difference built-up index in automatically mapping urban areas from TM imagery. *Int. J. Remote Sens.* 24, 583–594. <https://doi.org/10.1080/01431160304987>.

Zhang, C., Li, X., 2022. Land use and land cover mapping in the era of big data. *Land* 11, 1692. <https://doi.org/10.3390/land11101692>.

Zhang, H.K., Roy, D.P., 2017. Using the 500 m MODIS land cover product to derive a consistent continental scale 30 m Landsat land cover classification. *Remote Sens. Environ.* 197, 15–34. <https://doi.org/10.1016/j.rse.2017.05.024>.

Zhao, Q., Yu, L., Li, X., Peng, D., Zhang, Y., Gong, P., 2021. Progress and trends in the application of google earth and google earth engine. *Remote Sens* 13, 3778. <https://doi.org/10.3390/rs13183778>.

Zhao, S., Tu, K., Ye, S., Tang, H., Hu, Y., Xie, C., 2023. Land use and land cover classification meets deep learning: a review. *Sensors* 23, 8966. <https://doi.org/10.3390/s23218966>.

Zhao, Z., Islam, F., Waseem, L.A., Tariq, A., Nawaz, M., Islam, I.U., Bibi, T., Rehman, N.U., Ahmad, W., Aslam, R.W., Raza, D., Hatamleh, W.A., 2024. Comparison of three machine learning algorithms using google earth engine for land use land cover classification. *Rangel. Ecol. Manag.* 92, 129–137. <https://doi.org/10.1016/j.rama.2023.10.007>.

Zhu, Z., Zhou, Y., Seto, K.C., Stokes, E.C., Deng, C., Pickett, S.T.A., Taubenbock, H., 2019. Understanding an urbanizing planet: strategic directions for remote sensing. *Remote Sens. Environ.* 228, 164–182. <https://doi.org/10.1016/j.rse.2019.04.020>.

6. Appendix A: Contact Information for Key Project Personnel

Megan Cattau (Principal Investigator) Assistant Professor, Human Environment Systems, Boise State University, 1910 University Dr, Boise, ID 83725, USA. Email: megancattau@boisestate.edu



Megan Dolman (Student Investigator) PhD Candidate, Human Environment Systems, Boise State University, 1910 University Dr, Boise, ID 83725, USA. Email: megandolman@u.boisestate.edu

7. Appendix B: List of Completed/Planned Scientific/Technical Publications/Science Delivery

We have produced several products from this research, including manager-relevant deliverables, scientific manuscripts, and other products related to science delivery (Table 3). Our algorithm workflow and code are open source and available on Google Earth Engine and we will publish two manuscripts that will be related to this project, in addition to an ArcGIS StoryMaps to give a high-level overview of this project.

Table 3. Deliverables and products with description and status

Deliverable Type	Description	Delivery Dates
JFSP Final Report	Final report of the project for the JFSP	Complete
JFSP Progress Report	A JFSP progress report was submitted in December 2024.	Complete
JFSP Progress Report	A JFSP progress report was submitted in September 2023.	Complete
JFSP Project Overview	A modified version of the final report abstract within a one- to two-page format that communicates the key project outcomes and implications for management	Complete
Manager-Relevant Deliverable (a)	Annually-resolved remotely-sensed data products of contemporary infrastructural development	Complete

	<p>Dryad: https://doi.org/10.5061/dryad.mcvdnckb3</p> <p>Google Drive:</p> <p> Dolman.et.al.2025_AnnualClassifications</p>	
Manager-Relevant Deliverable (b)	<p>Summary guide to using the annually-resolved data products</p> <p> Summary Guide</p>	Complete
Manager-Relevant Deliverable (c)	<p>StoryMaps, created using ArcGIS StoryMaps to display the mapped products interactively, available at: https://arcg.is/n9e8T</p>	Complete
Manager-Relevant Deliverable (d)	Community partner meeting to present deliverables	Complete
Digitizing Definitions	<p>Definitions used for each of the six land use and land cover classes in the mapped built infrastructure (MBI) product. Available at: https://docs.google.com/document/d/1BjHnJ6LMfLvnrXwRKMUKWE3bTCwq3gweGDfl8iHdNc/edit?tab=t.0</p>	Complete
QGIS Digitizing Workflow	<p>Detailed workflow document that describes the process of manually digitizing imagery in QGIS and creating training data</p> <ul style="list-style-type: none"> - Includes an area of interest shapefile (Tetonia_Driggs_AOI) 	Complete
QGIS Digitizing Workflow Video	Walk-through video detailing how to generate digitize in QGIS, created by Savannah Canova	Complete
QGIS Print Layout	A walk-through video designed to demonstrate to use the print layout feature in QGIS to create a map	Complete
GEE Repository	<p>Open-source code for developing processing and detection Random Forest algorithms, classifying image stacks, and exploring change in land use and land cover over time. Available at: https://code.earthengine.google.com/?accept_repo=users/megdolman/SIAC_BuiltInfrastructureMapping</p>	Complete
Manuscript (1)	<p>A peer-reviewed manuscript presenting the algorithm development methods using Google Earth Engine, that includes evaluation of built infrastructure patterns in the Snake River Plain over time and a comparison of the mapped built infrastructure (MBI) product with other existing land use and land cover products. Published in <i>Remote Sensing Applications: Society and Environment</i> in January 2025. Available at: https://doi.org/10.1016/j.rsase.2025.101472</p>	Complete

Manuscript (2)	A review manuscript discussing WUI conceptualizations and definitions in the context of wildfire risk management. Emphasizes the value that remote-sensing products like MBI have for informing decision-making around wildfire risk to communities regardless of WUI designation. Will be submitted to <i>International Journal of Wildland Fire</i> for peer-review.	In progress
Conference Presentation (a)	Presented a poster at the Ecological Society of America annual meeting in Portland OR, August 2023	Complete
Conference Presentation (b)	Presented an oral presentation at the 7 th International Fire Behavior and Fuels Conference in Boise ID, April 2024	Complete
Conference Presentation (c)	Presented a poster at the National Cohesive Wildland Fire Management Strategy Workshop in Atlantic City NJ, November 2024	Complete
Graphical Representation (a)	An illustrated graphic outlining the algorithm development and image classification methods	Complete
Graphical Representation (b)	An illustrated graphic comparing existing land use land cover products in comparison to our mapped built infrastructure product	Complete
Artistic Representation	An original poem describing the JFSP funded project, presented at the National Cohesive Wildland Fire Management Strategy Workshop in Atlantic City NJ, November 2024	Complete

8. Appendix C: Metadata

Google Earth Engine (GEE) repository for MBI products is available at:

https://code.earthengine.google.com/?accept_repo=users/megdolman/SIAC_BuiltInfrastructureMapping

MBI products are publicly available at:

Dryad: <https://doi.org/10.5061/dryad.mcvdnckb3>

Google Drive:

https://drive.google.com/drive/folders/1faKaLfSwEiYhrunrSKAPdpGMEpogGR7V?usp=drive_link